Photoionization measurements for the iron isonuclear sequence Fe^{3+}, Fe^{5+}, and Fe^{7+}

M. F. Gharaibeh,[1,*] A. Aguilar,[1] A. M. Covington,[1] E. D. Emmons,[1] S. W. J. Scully,[1] R. A. Phaneuf,[1,†] A. Müller,[2] J. D. Bozek,[3] A. L. D. Kilcoyne,[3] A. S. Schlachter,[3] I. Àlvarez,[4] C. Cisneros,[4] and G. Hinojosa[4]

[1]*Department of Physics, University of Nevada, Reno, Nevada 89557-0220, USA*

[2]*Institut für Atom- und Molekülphysik, Universität Giessen, D-35392 Giessen, Germany*

[3]*Advanced Light Source, MS 7-100, Lawrence Berkeley National Laboratory Berkeley, California 94720, USA*

[4]*Centro de Ciencias Físicas, Universidad Nacional Autónoma de México, Apartado Postal 6-96, Cuernavaca 62131, Mexico*

(Received 11 February 2011; published 22 April 2011)

Cross sections for single photoionization of Fe^{3+}, Fe^{5+}, and Fe^{7+} ions were measured at spectral resolutions of 0.04, 0.15, and 0.13 eV, respectively, by merging mass- and charge-selected ion beams with a beam of monochromatized synchrotron undulator radiation. The measurements span photon energy ranges beginning at the ionization thresholds and extending several tens of electron volts to include the most important resonant contributions due to $3p$–nd transitions to autoionizing states. The photoion yield spectra are characterized by narrow resonances and also broad features in Fe^{3+} and Fe^{5+} that are believed to result from unresolved fast super-Coster-Kronig transitions following $3p$–$3d$ excitation. Absolute photoionization cross-section measurements were also performed using ion beams containing undetermined fractions of ions in their ground and metastable states. A Rydberg series attributed to $3p$–nd transitions from the $^2G_1$ metastablestate in Fe^{3+} was identified. The data are compared with recently published measurements on Fe^{3+} and Fe^{5+} using a similar technique at lower spectral resolution.

DOI: 10.1103/PhysRevA.83.043412 PACS number(s): 32.80.Fb, 32.80.Aa, 32.70.Cs

I. INTRODUCTION

Most of the known matter in the Universe is in ionic form, and much of our information about the Universe is carried by photons, which are dispersed and detected, for example, by the orbiting Chandra and XMM-Newton x-ray observatories [1]. While photons travel through stellar atmospheres and planetary nebulae, they are likely to interact with matter and therefore with ions. Since iron lies at the maximum of the nuclear stability curve, it is an astrophysically abundant and, hence, important element [2] that can serve as a diagnostic tool. Observing absorption features by iron ions in astrophysical environments and modeling the observed spectra can provide detailed insights into the physical properties of those environments [3,4]. Therefore iron ions are of great interest for astrophysical spectroscopy and models of stellar atmospheres, novae, and active galactic nuclei, as summarized by Nahar and Pradhan [3].

The photoionization process is also important in high-temperature plasma devices, such as controlled thermonuclear fusion reactors [5], and particularly in high-density inertially confined plasmas [6]. Of particular relevance are ions of the transition metals Ti, Mn, Fe, and Ni [7]. These are directly applicable to plasma cooling, transport, and confinement in experimental fusion devices. These metals are released as impurities from the walls of the fusion reactor, or deliberately as diagnostic tracer elements. Iron is a dominant impurity because it is often a major constituent of the fusion reactor chamber.

In plasma environments atoms can be found in a large variety of charge states. A strong motivation for studying ionization along isonuclear sequences, i.e., for different charge states of one element, is that the atomic structure changes significantly along the series as various filled subshells are opened. Thus, simple scaling laws are not expected to apply along isonuclear sequences. Obviously, absolute ionization and recombination cross-section data along the iron isonuclear sequence are required for modeling the properties and dynamics of many high-temperature plasmas [8]. Absolute cross sections for photoionization of iron ions are particulary important for the understanding of the behavior of hot high-density plasmas. They are especially required for the modeling of astrophysical environments and their absorption and emission characteristics.

Ionization of iron ions by electron impact has been extensively studied in crossed- and merged-beams experiments [9–15]. Photoionization measurements reported for iron include those made for neutral iron [16,17] using synchrotron radiation and an atomic-beam technique. Absolute single- and double-photoionization cross sections for Fe^+ were measured using a merged-beams technique at photon energies between 15.8 and 180 eV [18] and Fe^{4+} between 59 and 140 eV [19]. Photoionization of Fe^{2+} through Fe^{6+} has been measured recently from their single ionization thresholds up to 160 eV [20]. In a proof-of-principle experiment with trapped Fe^{14+} ions photoionization was studied in selected energy bins within the range 450–1100 eV [21]. Photoionization of Fe^{7+} has been explored theoretically as part of the Opacity Project [22] and Iron Project [3]. Calculations for $2p$–$3d$ excitations were reported by Zeng *et al.* [23]. Detailed resonance structure in the photoionization of Fe^{7+} has recently been calculated by Sossah *et al.* [24].

II. EXPERIMENT

The experiment was performed at the ion photon beam (IPB) endstation on undulator beamline 10.0.1 at the Advanced

*Present address: Department of Physics, Jordan University of Science and Technology, Irbid 22110, Jordan.

†phaneuf@unr.edu

Light Source (ALS). Since a detailed description of the experimental setup has been reported [25], only a brief description emphasizing details that are specific to the present investigation is presented here. Iron ions were produced from ferrocene [$Fe(C_5H_5)_2$] powder by the MIVOC (Metal Ions from VOlatile Compounds) method, which facilitates the production of metal ions under near-room-temperature conditions [26]. The vapor from this volatile compound was allowed to diffuse at a controlled rate into the plasma chamber of a compact all-permanent-magnet electron cyclotron-resonance (ECR) ion source [27].

An ion beam was extracted from the ECR ion source discharge by placing the plasma chamber at a positive potential of +6 kV. After downstream focusing, collimation, and differential pumping, a dipole magnet selected from this beam iron ions with the desired ratio of mass per charge. The ion beam was subsequently merged onto the axis of a counterpropagating photon beam by applying appropriate voltages to several electrostatic steering and focusing devices. The photon beam of monochromatized synchrotron undulator radiation and the ion beam were merged in ultrahigh vacuum over a common path of approximately 140 cm.

Downstream of the interaction region, the ion beam was demerged from the photon beam by a second dipole magnet that also separated the further-ionized iron product ions from the parent beam. These product ions were further directed by steering plates onto a single-particle detector that counted them with near-unit efficiency. The detector signal count rate was only partly due to photoionization events, since product ions were also produced by stripping collisions with residual gas molecules and surfaces. This background was subtracted by mechanically chopping the photon beam. For normalization, the primary ion beam current was collected in a Faraday cup and the photon flux was recorded by a calibrated silicon x-ray photodiode (IRD, AXUV-100) [28].

Absolute cross sections were determined by normalizing the photoion count rate to the measured primary ion beam current, to the photodiode current, and to the interaction volume determined by spatial overlap of the photon and ion beams. Two-dimensional ion and photon beam profile measurements along the merged path were carried out using two commercial rotating-wire beam-profile monitors and a translating-slit scanner. To maximize the count rate for spectroscopic measurements, product ions were collected from the entire 140-cm merged path. For absolute measurements, the product ions were energy-tagged by applying a potential of +1.5 kV to a central interaction region of known length (29.4 cm) within which the spatial overlap of the beams was well characterized. The demerger magnet and product-ion deflector were retuned to accept only these energy-tagged ion products. Because $^{56}Fe^{7+}$ has the same charge-to-mass ratio as $^{16}O^{2+}$, $^{54}Fe^{7+}$ was used for the absolute measurements.

Spectroscopic energy-scan measurements were taken by stepping the photon energy through a preset range of values at fixed energy resolution. Owing to the considerable time and effort required to carry out absolute measurements, they were preferentially performed at selected photon energies in regions where the photoion yield spectrum exhibited a smooth energy dependence. The $^{54}Fe^{7+}$ current was typically only 1 nA, making measurements of the small nonresonant photoionization cross section impractical. In this case, the absolute measurements were performed on resonances at the same resolution as the spectroscopic measurements. In all cases, the energy-scan measurements were normalized to the absolute measurements by fitting a first- or second-order polynomial to their measured ratio as a function of photon energy. The systematic uncertainties in the determinations of the absolute cross-section scales are estimated at a confidence level comparable to 90% on statistical uncertainties to be ±25% for the Fe^{3+} and Fe^{5+} measurements and ±30% for Fe^{7+}.

III. RESULTS

A. Photoionization of Fe^{3+}

The electronic ground-state configuration of Fe^{3+} is $[Ar]3d^5$ and within the resulting manifold the $^6S_{5/2}$ state has the lowest energy. A half-filled $3d$ subshell complicates the electronic structure such that, in addition to the ground state, the $[Ar]3d^5$ configuration gives rise to 15 long-lived metastable states. The $[Ar]3d^44s$ configuration also has 23 known metastable states according to the National Institute of Standards and Technology (NIST) atomic spectra database [29]. Metastable states are well known to be populated in an ECR ion source discharge and are expected to be present in the primary ion beam if their lifetimes are comparable to or greater than their flight time in the apparatus ($\sim 10^{-5}$ s). Thus the primary Fe^{3+} ion beam consists of an undetermined admixture of ions in the ground state and in metastable states, and the detected photoions can originate from any of these states. While this enriches the measured photoion yield spectrum, it makes the data analysis challenging and complicates any comparison with theoretical calculations.

The Fe^{4+} product ion yield from photoionization of Fe^{3+} was measured as the photon energy was stepped from 38 to 83.5 eV at 4-meV intervals at a fixed energy resolution of 40 meV. The photon energy scale was calibrated *in situ* by measuring the He^+ ionization threshold (54.41778 eV) [29] and the C^+ $[2s^22p(^2P)\text{-}2s^2p(^3P)4p(^2D)]$ photoionization resonance (26.879 ±0.015 eV) [30]. The resulting uncertainty in the energy scale is estimated to be ±0.016 eV. Absolute cross-section measurements were performed at discrete photon energies where narrow resonances were absent in the photoion yield spectrum and were used to place the energy-scan data on an absolute scale. The resulting cross section for photoionization of Fe^{3+} is shown in the upper panel in Fig. 1, where the absolute measurements are indicated by open circles with error bars. The lower panel is a similar merged-beams measurement performed recently at the ASTRID synchrotron in Denmark [20]. In this energy range the photon energy bandpass in the ASTRID measurements increases smoothly between 0.14 and 0.62 eV. Small differences between the two measurements of the nonresonant continuum cross section due to direct photoionization are attributed to differing populations of metastable states in the Fe^{3+} primary ion beams, since in the ASTRID experiments Fe ions were produced by heating iron metal in a micro-oven inserted into the ECR ion source. Narrow resonances are much more prominent in the present measurements because of the increased energy resolution.

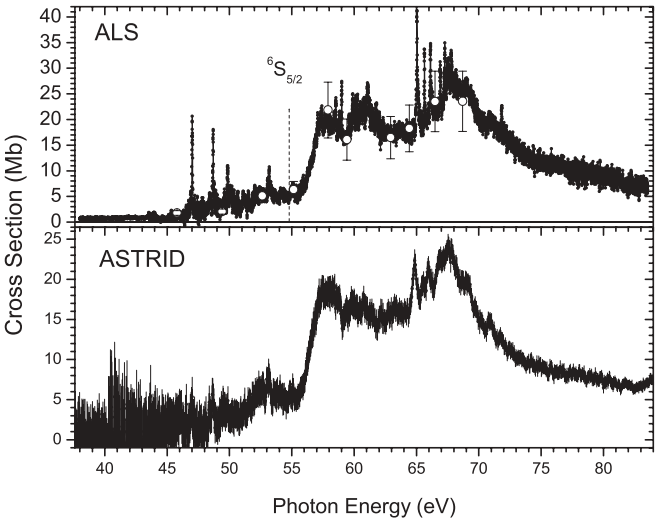

FIG. 1. Cross-section measurements for single photoionization of Fe^{3+}. The upper panel shows the present measurements at ALS in the energy range 38–84 eV at a fixed photon energy resolution of 0.04 eV. Absolute measurements are shown by open circles with error bars, to which the energy scan data are normalized. The vertical dashed line represents the tabulated ionization threshold of the $^6S_{5/2}$ ground state at 54.80 eV. The lower panel shows the absolute cross section measured at ASTRID in the same energy range at a photon energy resolution ranging from 0.14 to 0.62 eV [20].

In the region below the $3d^5(^6S_{5/2})$ ground-state ionization threshold at 54.80 eV there is evidence of a Rydberg series due to excitation from the $3d^5(^2G_1)$ metastable state to the states $3d^4(^1G_1)np(^2F^0)$, where n is the principal quantum number. This series starting from $n = 7$ is shown in Fig. 2. The spectroscopic energy limit ($n = \infty$) of this series is 53.36 eV [29], which corresponds to the difference between the ionization

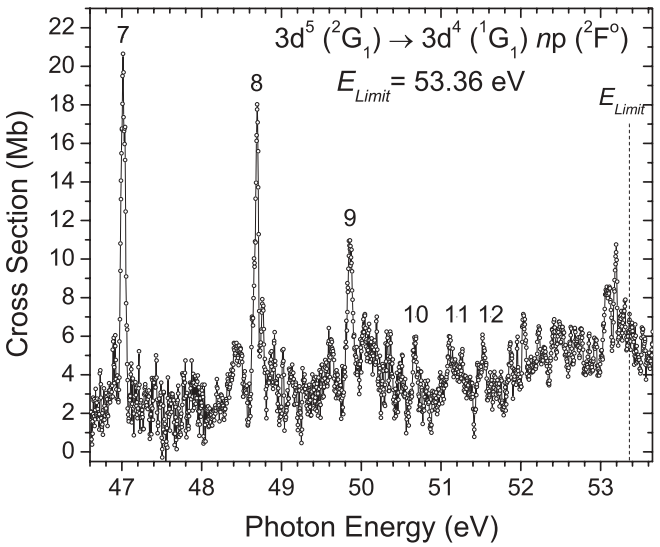

FIG. 2. Photoionization of Fe^{3+} in the region below the ground-state threshold on an expanded energy scale showing the Rydberg series attributed to autoionizing transitions from $3d^5(^2G_1)$ to $3d^4(^1G_1)np(^2F^0)$, where n is the principal quantum number starting from $n = 7$. The spectroscopic energy limit of this Rydberg series is 53.36 eV [29] (indicated by the vertical dashed line).

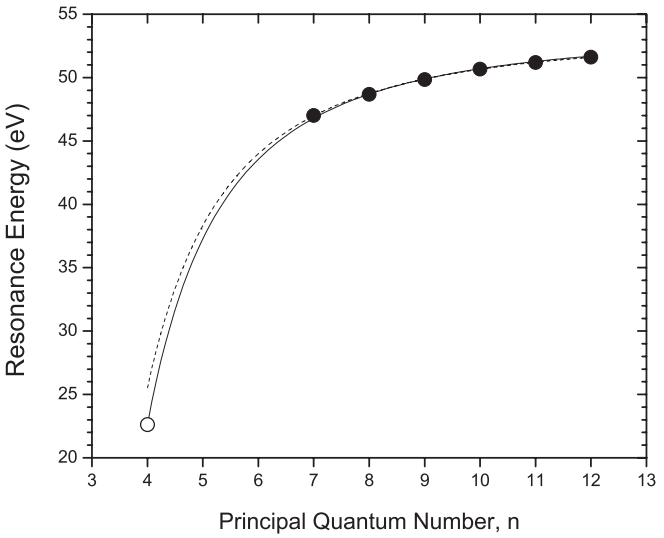

FIG. 3. Rydberg fits for the $3d^4(^1G_1)np(^2F^0)$ series from the $^2G_1$ metastable state of Fe^{3+}. The solid curve was obtained by including the bound state ($n = 4$) transition [29] (indicated by the open circle) in the fit, while the dashed curve was obtained without this bound transition.

potentials of the states $3d^5(^2G_1)$ and $3d^4(^1G_1)$. The measured resonance energies for this series are plotted versus n in Fig. 3, which shows a fit of the quantum-defect form of the Rydberg formula. The solid curve is the fit obtained by including the tabulated energy for the bound transition for $n = 4$ [29] (indicated by an open circle), while the dashed curve is obtained without this bound-bound transition. Table I presents the fitting parameters for the curves. The internal consistency of the data for the bound and autoionizing levels is considered to be evidence for the assignment of this Rydberg series. The two curves differ because the quantum defect δ_n accounts for core electron screening of the nuclear charge and depends on n. The δ_n values for each n level calculated from the experimentally measured E_n using the Rydberg formula are presented in Table II and Fig. 4, where the series limit has been fixed to the spectroscopic value of 53.36 eV. The estimated uncertainties of the resonance energies are larger for $n = 11$ and $n = 12$ because additional resonances are evident in the energy ranges where they occur, making their assignments less accurate.

Figure 5 presents a measurement of the first resonance in this Rydberg series ($3p$–$7d$) at higher spectral resolution, showing it to be a doublet. Since the fine-structure splitting of

TABLE I. Rydberg fit parameters used to generate the two curves in Fig. 3.

	Series limit, E_{limit} (eV)	Quantum defect, δ
With the $n = 4$ bound state included[a]	53.611 ± 0.048	1.35 ± 0.01
With the $n = 4$ bound state excluded[a]	53.470 ± 0.031	1.21 ± 0.03

[a]Rydberg constant $R = 13.605\,576\,52$ eV, nuclear charge $Z = 26$, number of core electrons, $N = 22$.

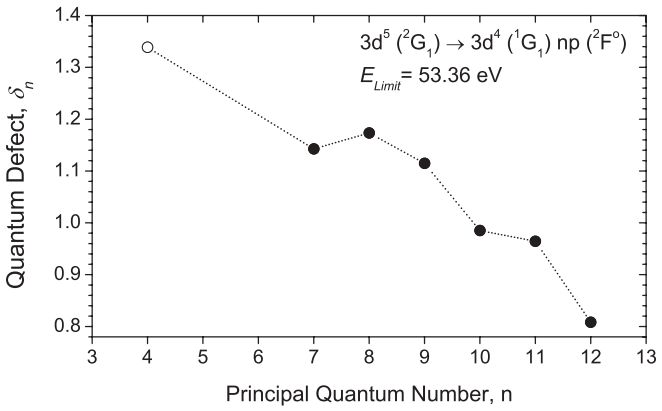

FIG. 4. Plot of quantum defects δ_n vs principal quantum number n for the Rydberg series $[\mathrm{Ar}]3p^4(^1G_1)np(^2F^0)$ from the $^2G_1$ metastable state of Fe^{3+}. The open circle represents the transition to the $n = 4$ bound state [29]. The dotted line just connects the data points.

the initial state is reported to be less than 1 meV [29], it was conjectured that the doublet may be due to the fine structure of the $3d^47p(^2F^0)$ final state. The shape of a measured resonance line profile is expected to be a convolution of the instrument function (a Gaussian) with the natural line profile (a Lorentzian), called a Voigt profile [31]. By fitting Voigt profiles to these lines, the measured separation between the $3d^47p(^2F^0_{7/2})$ and $3d^47p(^2F^0_{5/2})$ levels was determined to be 27 meV. By comparison, the energy separation of the $3d^44p(^2F^0_{7/2})$ and $3d^44p(^2F^0_{5/2})$ bound levels is reported to be 35 meV [29]. If the observed splitting is due to the fine structure, it should also be resolved in the next resonance ($n = 8$), but a high-resolution measurement of this resonance (not shown) did not show this doubling.

To interpret these high-resolution measurements, the Cowan atomic structure code [32] was used to estimate the energy separation due to the fine structure of the $3d^4(^1G_1)np(^2F^0)$ states along the investigated Rydberg series. For $n = 4$ the Cowan code predicts the splitting to be 39 meV (close to the tabulated value of 35 meV); the splitting is 7 meV for $n = 7$ and decreases with n.

TABLE II. The principal quantum numbers n, experimentally measured resonance energies, and calculated quantum defects δ_n for the $3d^4(^1G_1)np(^2F^0)$ series from the $^2G_1$ metastable state of Fe^{3+}. The entry in parentheses for $n = 4$ is the tabulated bound-state transition value as is the series limit [29].

Principal quantum number, n	Rydberg series resonance energy (eV)	Quantum defect, δ
4	(22.624)	1.34
7	47.015 ± 0.020	1.14
8	48.689 ± 0.020	1.17
9	49.859 ± 0.020	1.11
10	50.681 ± 0.020	0.99
11	51.199 ± 0.060	0.96
12	51.622 ± 0.100	0.81
⋮		
∞	53.360	

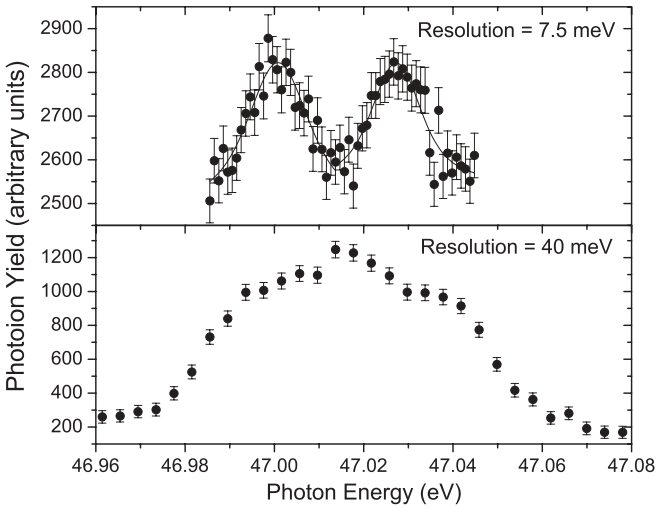

FIG. 5. Comparison of measurements of the resonance corresponding to the transition $3d^5(^2G_1)$ to $3d^47p(^2F^0)$ in Fe^{3+} at experimental energy resolutions ΔE of 40 and 7.5 meV. The curve is a fit of Voigt profiles to the two resonance features.

Thus the fine structure is not expected to be resolvable for $n = 7$ at the experimental resolution of 7.5 meV. These results suggest that only one of these two resonances belongs to the $3d^4(^1G_1)np(^2F^0)$ Rydberg series from $3d^5(^2G_1)$ and the other may be associated with photoexcitation of Fe^{3+} in a different initial metastable state.

The three broad features centered near 58, 61, and 68 eV may be due to unresolved $3p$–$3d$ excitations from the ground state and from the numerous metastable states. Autoionization of the $3p^53d^6$ configuration is known to be extremely fast via super-Coster-Kronig transitions [33] and the associated resonances have large widths. The importance of $3p$–$3d$ excitations has been noted in photoionization such as in Cr, Cr^+, Mn, and Mn^+ [34,35] and Ca^+ [36], Sc^{2+} [37,38], and Ti^{3+} [39]. Reviews addressing $3p$–$3d$ excitations in atoms and ions with an open d subshell were provided by Martins *et al.* [17] and Kjeldsen [40].

B. Photoionization of Fe^{5+}

The electronic ground-state configuration of Fe^{5+} is $[\mathrm{Ar}]3d^3$ and within the resulting manifold the $^4F_{3/2}$ state has the lowest energy. In addition to the ground state, the $[\mathrm{Ar}]3d^3$ configuration gives rise to seven long-lived metastable states, and the $[\mathrm{Ar}]3d^24s$ configuration has six known metastable states. Thus, as for Fe^{3+}, the Fe^{5+} primary ion beam is expected to consist of an admixture of ions in the ground state and in metastable states, and the detected photoions can originate from any of these states whose lifetimes are comparable to or greater than the ion flight time in the apparatus ($\sim 10^{-5}$ s).

The Fe^{6+} product ion yield was measured as the photon energy was stepped from 87 to 142 eV at 0.020-eV intervals with a fixed energy resolution of 0.150 eV. The photon energy scale was calibrated using a gas cell on a separate branch of ALS Beamline 10.0. The calibration employed the Ar ($2p_{3/2}$-$4s$) resonance in second order on the grating (122.195 ± 0.010 eV) and the Kr ($3d_{5/2}$-$5p$) resonance (91.200 ± 0.010 eV) in first order [41]. The uncertainty in the photon

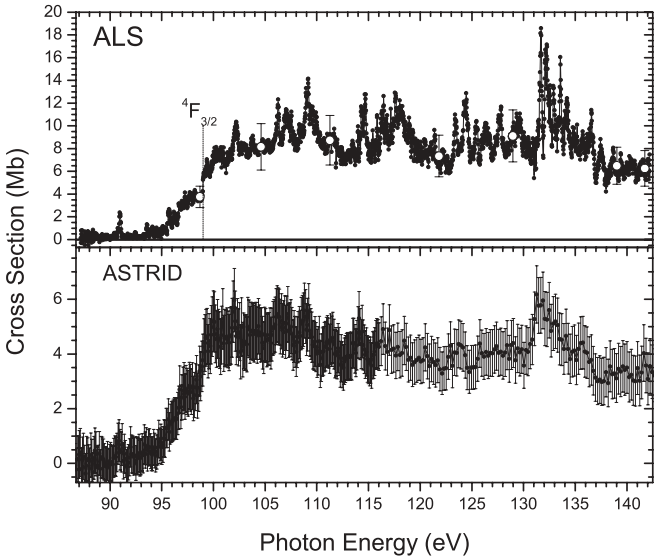

FIG. 6. Single photoionization of Fe^{5+} in the energy range 87–142 eV. The upper panel shows the present ALS measurements made at a fixed spectral resolution of 0.15 eV. Absolute cross-section measurements are shown by open circles with error bars, to which the energy scan data are normalized. The vertical dashed line represents the tabulated ionization threshold of the $^4F_{3/2}$ ground state at 99.063 eV. The lower panel shows the photoionization cross section measured at ASTRID at lower spectral resolution in the same energy range [20].

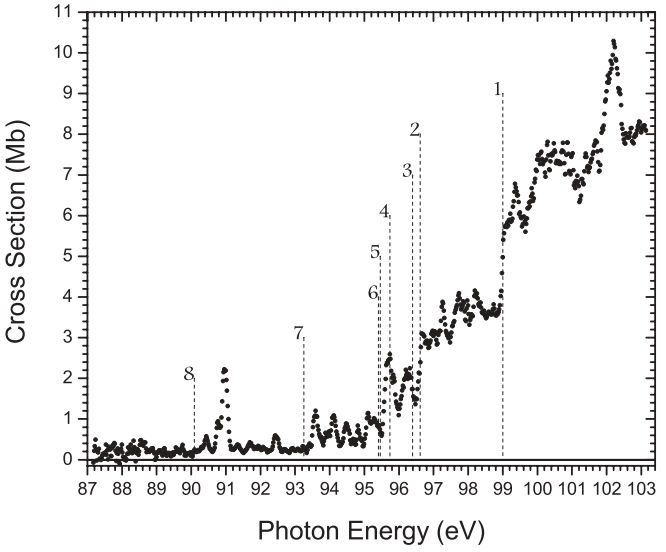

FIG. 7. Absolute cross-section measurement for single photoionization of Fe^{5+} on an expanded energy scale in the range where the ionization thresholds of the eight [Ar]$3d^3$ terms are expected [29] (indicated by dashed vertical lines). The numbers labeling these thresholds are identified in Table III, with 1 representing the $^4F_{3/2}$ ground state.

energy scale is estimated to be ±0.014 eV. At each energy, the photoion counts were normalized to the photon flux and primary ion beam current. The Fe^{5+} measurements span the energy range where absorption near the L $(2p)$ edge of Si at 99.8 eV and of SiO_2 at 105.4 eV [28] causes sharp decreases in the photodiode efficiency. Corrections were made to the photon flux recorded by the photodiode at energies near these features to remove corresponding artifacts in the normalized photoion yield. Absolute cross-section measurements were performed with well-characterized beams at discrete photon energies where resonances were absent in the photoion yield spectrum.

The present experimental results for single photoionization of Fe^{5+} at a fixed spectral resolution of 0.15 eV are shown in the upper panel of Fig. 6, where the absolute cross-section measurements are indicated by open circles with error bars. The lower panel shows the measurement performed recently at ASTRID [20], for which the energy bandpass is described to increase smoothly from 0.35 to 2.25 eV. In this case the continuum photoionization cross section underlying the resonance features differs considerably between the two measurements. The integral oscillator strengths determined by integrating the measured cross sections over this energy range differ by a factor of 2. Since the energy dependencies of the photoionization measurements also differ, this disagreement may be at least in part attributable to differing populations of metastable states in the Fe^{5+} primary ion beams. As noted, iron ions were produced for the ALS experiments by evaporating ferrocene at room temperature, whereas metallic iron was evaporated at 1300 °C for the ASTRID measurements.

The broad feature above the ground-state threshold underlying the narrow resonance structure is similar to that observed in photoionization of Fe^{3+}. For ground-state Fe^{5+} ions, $3p$–$3d$ excitations populate only bound states and do not lead to ionization. However, the feature may result from unresolved $3p$–$3d$ excitations from metastable states of Fe^{5+}, resulting in extremely fast super-Coster-Kronig transitions and broad, unresolved resonances [33].

Figure 7 expands the energy region where the ionization thresholds of the eight [Ar]$3d^3$ states (all long lived) are predicted, based on NIST tabulated spectral data [29]. Underlying the resonance structure, the measurements show distinct threshold steps at the energies labeled 1 and 2, closely matching the tabulated values for the $^4F_{3/2}$ ground state and the ^4P metastable state, respectively. Significant ionization occurs at photon energies below the ground-state threshold, indicating substantial population of metastable states in the Fe^{5+} ion beam. Steps due to the other predicted thresholds are less evident in the data, because they are smaller and/or obscured by nearby resonances. Table III compares the experimental energies of these steps with the corresponding tabulated values. The uncertainties in the measured threshold energies were estimated from fits to these steps and from the photon energy calibration using the gas cell and represent their quadrature sum. The fractional population of the $^4F_{3/2}$ ground state may be estimated from the difference in the measured total cross section just below and above this threshold step (2.34 Mb) and by comparing that value with the direct photoionization cross-section calculation by Berrington and Ballance [22] for the ground-state at threshold (7.28 Mb). The resulting fraction (0.32 ± 0.08) is presented in Table III, the uncertainty reflecting that of the absolute cross-section measurement.

TABLE III. Comparison between the ionization threshold energies from this work and the NIST tabulated values [29]. The population fraction of the ground state estimated from the measured cross section is indicated in the last column.

Number	Ionization potential (eV)		Term	Population fraction
	This work	NIST		
1	98.985 ± 0.015	99.000	$^4F_{3/2}$	0.32 ± 0.08
2	96.628 ± 0.015	96.614[a]	^4P	
3		96.396[a]	G	
4		95.738[a]	^2P	
5		95.461[a]	$^2D_2$	
6		95.406[a]	^2H	
7		93.249[a]	^2F	
8		90.092[a]	$^2D_1$	

[a]Term energy weighted statistically by $(2S + 1)(2L + 1)$.

C. Photoionization of Fe^{7+}

Fe^{7+} is potassium-like with the electronic ground-state configuration [Ar]3d and the ground-state term $^2D_{3/2}$. It is within a sequence of ions that has been addressed previously in detail [37–39,42,43]. The [Ar]3d configuration gives one $^2D_{5/2}$ metastable state. According to the NIST atomic spectra database [29], the ground-state ionization potential is 151.060 eV and the ^2D fine-structure splitting is 0.228 eV. The configuration [Ar]4s gives a high-lying $^2S_{1/2}$ metastable state, which is not tabulated. The Cowan atomic structure code [32] predicts the $^2S_{1/2}$ ionization threshold to be 52.623 eV below that of the ground state. The $^{56}Fe^{8+}$ product ion yield from single photoionization of $^{56}Fe^{7+}$ was measured as the photon energy was stepped from 150 to 172.5 eV at 0.01-eV intervals with a fixed energy resolution of 0.126 eV. The photon energy scale was calibrated with a gas cell on a separate branch of ALS Beamline 10.0 using the CO_2 (C: 1s-3s) resonance (292.74 $\pm$ 0.02 eV) in first and second order [44] and the SF_6 (S: $2p_{1/2}$-t_{2g}) resonance (184.54 $\pm$ 0.05 eV) in first order [45]. The resulting uncertainty in the energy scale is estimated to be $\pm$0.057 eV.

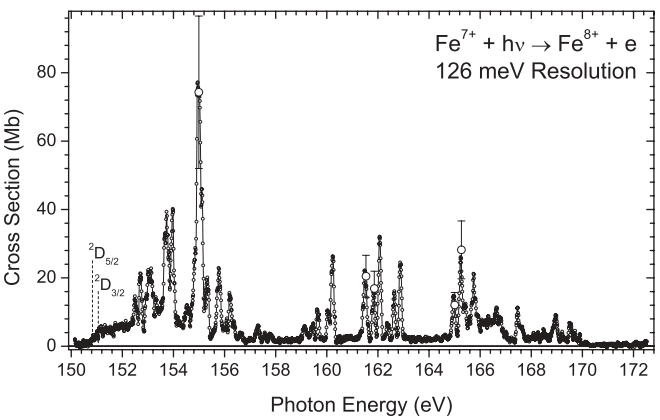

FIG. 8. Absolute cross section for photoionization of Fe^{7+} in the energy range 150–172.5 eV measured at a spectral resolution of 0.126 eV. Absolute cross-section measurements are shown by open circles with error bars, to which the energy scan data are normalized. The vertical dashed lines represent the ionization thresholds of the $^2D_{3/2}$ ground state and the $^2D_{5/2}$ metastable state.

Possible contamination of the $^{56}Fe^{7+}$ beam with $^{16}O^{2+}$ ions was estimated by comparing the ratio of the apparent $^{56}Fe^{7+}$ and $^{55}Fe^{7+}$ ion-beam currents to the natural relative fractional abundances of these isotopes. The fraction of $^{56}Fe^{7+}$ was estimated to be 57%. The presence of a significant fraction of $^{16}O^{2+}$ ions in the primary beam had no effect on the measured relative photoion yield spectrum, since $^{16}O^{3+}$ and $^{56}Fe^{8+}$ products do not reach the photoion detector at the same settings of the demerger magnet and signal ion deflector. Their only effect was an initially incorrect normalization of the photoion yield spectrum to the primary ion beam current. However, as previously noted, the photoion yield spectrum was subsequently renormalized to absolute cross-section measurements performed using $^{54}Fe^{7+}$ as the primary ion beam. These measurements were performed on resonances because of the low ion beam current and small nonresonant photoionization cross section. The resulting cross section for

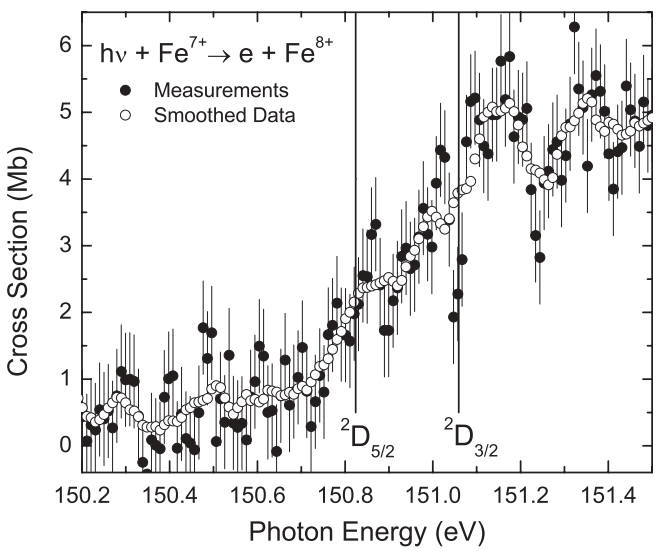

FIG. 9. Measurements of single photoionization of Fe^{7+} on an expanded energy scale in the region of the [Ar]3$d^2D_{3/2}$ ground state and $^2D_{5/2}$ metastable state ionization thresholds. The vertical lines indicate the tabulated values in the NIST atomic spectra database [29]. Solid circles represent the energy-scan measurements and open circles are the same measurements to which five-point Savitsky-Golay smoothing [46] was applied to reduce the statistical fluctuations.

single photoionization of Fe^{7+} is shown in Fig. 8, where the absolute measurements are indicated by open circles with error bars.

Figure 9 expands the energy region where the ionization thresholds of the $[Ar]3d^2D_{3/2}$ and $^2D_{5/2}$ states are predicted to occur. The measurements are consistent within the estimated experimental uncertainty of ± 0.057 eV with steps in the photoionization cross section at the threshold energies of 150.821 and 151.060 eV, as tabulated in the NIST atomic spectra database [29]. The nonzero cross section below the $^2D_{5/2}$ threshold is attributed to a small fraction of the Fe^{7+} ion beam in the $[Ar]4s^2S_{1/2}$ metastable state, whose ionization threshold is predicted to be 98.436 eV [29].

Theoretical calculations of cross sections for photoionization of Fe^{7+} based on the R-matrix method in LS coupling were available for comparison in the TOPbase astrophysical database [47]. To perform a comparison with experiment, the theoretical cross section was convoluted with a Gaussian function of FWHM = 0.126 eV to represent the experimental energy resolution. The theoretical cross sections for the three initial states were statistically weighted by $(2S + 1)(2L + 1)$ and summed to approximate the initial-state populations in the ion beam. Since the TOPbase predicted ionization potential of the ^2D ground state was lower than the NIST tabulated value by 4.059 eV, the TOPbase data were shifted upward by that amount. The resulting comparison with experiment is presented in Fig. 10. Significant differences between the TOPbase and the experimental data are evident in the positions, strengths, and numbers of resonances. Integrating the apparent experimental cross section over the energy range 150–172 eV gives an effective oscillator strength of 1.31 ± 0.39, which compares to a value of 0.25 for the TOPbase calculation. It is worth noting in this context that time-reversed photoionization of Fe^{7+} has been studied experimentally by storing Fe^{8+} ions in a heavy-ion storage ring and exposing the ions to a target of free electrons [48]. Strong recombination resonances were observed in an electron-ion collision energy range 0–20 eV, which corresponds to the present photon energies from the threshold at about 151–171 eV. Calculations employing state-of-the-art theory for the description of $Fe^{8+} + e$ recombination resonances did not reproduce the details of the measurement with its distribution of narrow peaks in the investigated energy range but produced total resonance strengths similar to those observed in the experiment [48].

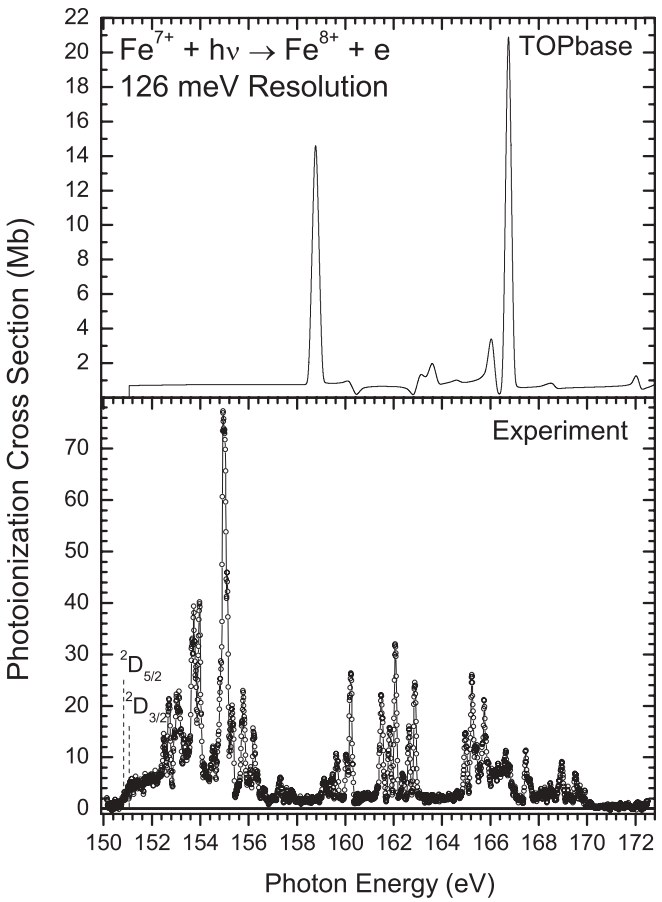

FIG. 10. Comparison of absolute cross-section measurements for photoionization of Fe^{7+} with the TOPbase theoretical data, shifted by +4.059 eV to match the ground-state ionization potential with the NIST tabulated value and convoluted with a Gaussian of FWHM = 0.126 eV to simulate the experimental energy resolution.

IV. SUMMARY AND CONCLUSIONS

Absolute cross-section measurements for single photoionization of Fe^{3+}, Fe^{5+}, and Fe^{7+} are strongly influenced by undetermined populations of metastable states in the primary ion beams, which complicate their interpretation and comparisons with theory and other measurements. The present experiments were performed at higher spectral resolution than previously published results for Fe^{3+} and Fe^{5+}, and they reveal additional evidence of structure due to excitation of autoionizing states. The observed resonance structure is attributed mainly to $3p$–nd transitions with $n \geqslant 3$ for Fe^{3+}, $n \geqslant 4$ for Fe^{5+}, and $n \geqslant 4$ for Fe^{7+}.

In the case of Fe^{3+}, a Rydberg series of $3d$-np resonances originating from the metastable state $3d^5(^2G_1)$ was identified and quantum defects were determined for $7 \leqslant n \leqslant 12$. Three broad features centered near 58, 61, and 68 eV are attributed to unresolved $3p$–$3d$ excitations from the ground state and from the numerous metastable states. Such $\Delta n = 0$ transitions populate autoionizing states that decay extremely rapidly by super-Coster-Kronig transitions, producing broad resonances in photoionization. The present data are in general qualitative and quantitative agreement with recently reported measurements at ASTRID and reveal additional resonance features because of their greater spectral resolution.

In the case of Fe^{5+}, the experimental data show distinct threshold steps at energies closely matching the NIST tabulated values for the $^4F_{3/2}$ ground state and the ^4P metastable state. The fractional population of the $^4F_{3/2}$ ground state was estimated to be 0.32 ± 0.08. The present ALS measurements are in fair qualitative agreement with recently reported measurements at ASTRID and reveal additional resonance features because of their higher spectral resolution. Oscillator strengths obtained by integrating the measured cross sections in the energy range 90–145 eV differ by a factor of 2, which exceeds their combined absolute uncertainties. The disagreement may result from differing populations of metastable states in the primary ion beams. Consistent with such an explanation is the

fact that the energy dependencies of the continua underlying the resonance structure differ considerably more than in the case of of Fe^{3+}.

In the Fe^{7+} measurement, steps in the single photoionization cross section are evident at the predicted ionization threshold energies of the [Ar]$3d\,^2D_{3/2}$ and $^2D_{5/2}$ states. The cross-section measurements do not compare favorably with the theoretical data in the TOPBase astrophysical database for this quasi-one-electron ion, emphasizing the significant challenge presented to theorists in calculating the structure and dynamics of ions with open $3d$ subshells.

The current measurements emphasize the complications introduced by the population of metastable states in the primary ion beam in merged-beams experiments, particularly those involving multiply charged ions. This makes comparisons between experiment and theory less definitive. Methods to quench metastable states by collisions with a gas have been successful only in a few select cases where electron-capture cross sections for ions in the metastable and ground states differ appreciably [49]. Trapping the ions for a period longer than the mean lifetimes of the metastable levels before making a photoionization measurement offers another promising approach to this problem [50].

ACKNOWLEDGMENTS

This research was supported by the Chemical Sciences, Geosciences and Biosciences Division, Office of Basic Energy Sciences, Office of Science, US Department of Energy, under Grant No. DE-FG02-03ER15424. Additional funding was provided by the Office of Basic Energy Sciences, US Department of Energy, under Contract No. DE-AC03-76SF0098, by the Deutsche Forschungsgemeinschaft, and by CONACYT, Mexico.

[1] F. B. S. Paerels and S. M. Kahn, Annu. Rev. Astron. Astrophys. **41**, 291 (2003).
[2] K. Langanke and M. Wiescher, Rep. Prog. Phys. **64**, 1657 (2001).
[3] S. Nahar and A. K. Pradhan, Astron. Astrophys. **437**, 345 (2005).
[4] D. Flower, *Atoms in Astrophysics* (Plenum, New York, 1983).
[5] R. McWhirter and H. Summers, *Applied Atomic Collision Physics* (Academic, New York, 1983).
[6] E. I. Moses, R. N. Boyd, B. A. Remington, C. J. Keane, and R. Al Ayat, Phys. Plasmas **16**, 041006 (2009).
[7] J. Colgan, D. M. Mitnik, and M. S. Pindzola, Phys. Rev. A **63**, 012712 (2000).
[8] A. Müller, Adv. At. Mol. Phys. **55**, 293 (2008).
[9] R. G. Montague and M. F. A. Harrison, J. Phys. B **17**, 2707 (1984).
[10] D. C. Gregory, F. W. Meyer, A. Müller, and P. Defrance, Phys. Rev. A **34**, 3657 (1986).
[11] D. C. Gregory, L. J. Wang, F. W. Meyer, and K. Rinn, Phys. Rev. A **35**, 3256 (1987).
[12] J. Linkemann, A. Müller, J. Kenntner, D. Habs, D. Schwalm, A. Wolf, N. R. Badnell, and M. S. Pindzola, Phys. Rev. Lett. **74**, 4173 (1995).
[13] M. Stenke, K. Aichele, U. Hartenfeller, D. Hathiramani, M. Steidl, and E. Salzborn, J. Phys. B **32**, 3627 (1999).
[14] M. Stenke, U. Hartenfeller, K. Aichele, D. Hathiramani, M. Steidl, and E. Salzborn, J. Phys. B **32**, 3641 (1999).
[15] M. Hahn *et al.*, Astrophys. J. **729**, 76 (2011).
[16] H. Feist, M. Feldt, C. Gerth, M. Martins, P. Sladeczek, and P. Zimmermann, Phys. Rev. A **53**, 760 (1996).
[17] M. Martins, K. Godehusen, T. Richter, P. Wernet, and P. Zimmermann, J. Phys. B **39**, R79 (2006).
[18] H. Kjeldsen, B. Kristensen, F. Folkmann, and T. Andersen, J. Phys. B **35**, 3655 (2002).
[19] J. M. Bizau, C. Blancard, D. Cubaynes, F. Folkmann, D. Kilbane, G. Faussurier, H. Luna, J. L. Lemaire, J. Blieck, and F. J. Wuilleumier, Phys. Rev. A **73**, 020707 (2006).
[20] N. El Hassan, J. M. Bizau, C. Blancard, P. Cossé, D. Cubaynes, G. Faussurier, and F. Folkmann, Phys. Rev. A **79**, 033415 (2009).
[21] M. Simon *et al.*, Phys. Rev. Lett. **105**, 183001 (2010).
[22] K. A. Berrington and C. Ballance, J. Phys. B **34**, 2697 (2001).
[23] J. Zeng, G. Dong, G. Zhao, and J. Yuan, J. Phys. B **37**, 2529 (2004).
[24] A. M. Sossah, H.-L. Zhou, and S. T. Manson, Phys. Rev. A **82**, 043416 (2010).
[25] A. M. Covington *et al.*, Phys. Rev. A **66**, 062710 (2002).
[26] H. Koivisto, J. Ärje, and M. Nurmia, Nucl. Instrum. Methods Phys. Res. B **94**, 291 (1994).
[27] F. Broetz, R. Trassl, R. W. McCullough, W. Arnold, and E. Salzborn, Phys. Scr. **92**, 278 (2001).
[28] E. M. Gullikson, R. Korde, L. R. Canfield, and R. E. Vest, J. Electron Spectrosc. Relat. Phenom. **80**, 313 (1996).
[29] Y. Ralchenko, A. E. Kramida, J. Reader, and NIST-ASD Team, Atomic spectra database, version 4, [http://www.nist.gov/physlab/data/asd.cfm].
[30] H. Kjeldsen, J. E. Hansen, F. Folkmann, H. Knudsen, J. B. West, and T. Andersen, Astrophys. J. Supp. Ser. **135**, 285 (2001).
[31] E. McDaniel, *Atomic Collisions: Electron & Photon Projectiles* (Wiley, New York, 1989).
[32] R. Cowan, *The Theory of Atomic Structure and Spectra* (University of California Press, Berkeley, 1981).
[33] N. Stolterfoht, Phys. Rep. **146**, 315 (1987).
[34] J. W. Cooper, C. W. Clark, C. R. Cromer, T. B. Lucatorto, B. F. Sonntag, E. T. Kennedy, and J. T. Costello, Phys. Rev. A **39**, 6074 (1989).
[35] J. T. Costello, E. T. Kennedy, B. F. Sonntag, and C. W. Clark, Phys. Rev. A **43**, 1441 (1991).
[36] J. E. Hansen and P. Quinet, J. Electron Spectrosc. Relat. Phenom. **79**, 307 (1996).
[37] S. Schippers *et al.*, Phys. Rev. A **67**, 032702 (2003).
[38] S. Schippers *et al.*, Phys. Rev. Lett. **89**, 193002 (2002).
[39] S. Schippers *et al.*, J. Phys. B **37**, L209 (2004).
[40] H. Kjeldsen, J. Phys. B **39**, R325 (2006).
[41] G. C. King, M. Tronc, F. H. Read, and R. C. Bradford, J. Phys. B **10**, 2479 (1977).

[42] I. C. Lyon, B. Peart, K. Dolder, and J. B. West, J. Phys. B **20**, 1471 (1987).
[43] H. Kjeldsen, F. Folkmann, F. Innocenti, L. Zuin, and J. E. Hansen, J. Phys. B **35**, L375 (2002).
[44] M. Tronc, G. C. King, and F. H. Read, J. Phys. B **12**, 137 (1979).
[45] R. N. S. Sodhi and C. E. Brion, J. Electron Spectrosc. Relat. Phenom. **34**, 363 (1984).
[46] A. Savitsky and M. J. E. Golay, Anal. Chem. **36**, 1627 (1964).
[47] C. Mendoza, C. Zeippen, A. Pradhan, and F. Delahaye, TOPbase, available online from [http://cdsweb.u-strasbg.fr/topbase/topbase.html].
[48] E. W. Schmidt *et al.*, Astron. Astrophys. **492**, 265 (2008).
[49] H. Kjeldsen, B. Kristensen, R. L. Brooks, F. Folkmann, H. Knudsen, and T. Anderson, Astrophys J. Suppl. Ser. **138**, 219 (2008).
[50] R. Thissen, J. M. Bizau,C. Blancard, M. Coreno, C. Dehon, and P. Francheschi, Phys. Rev. Lett. **100**, 223001 (2008).